Electronic Supplementary Material (ESI) for Dalton Transactions.
This journal is © The Royal Society of Chemistry 2021

Electronic Supplementary Information

for

Hydrogen Bonding to Metals as a Probe for Inverted Ligand Field

*Alberto Pérez-Bitrián, Miguel Baya, José M. Casas, Antonio Martín, and Babil Menjón**

- 1. Experimental section and spectroscopic characterization S1
- 2. Crystal data and structure refinement S18
- 3. Computational details S24
- 4. Notes and references S27

1. Experimental Section and Spectroscopic Characterization

General Procedures and Materials. Unless otherwise indicated, the reactions and manipulations were carried out under purified argon by using Schlenk techniques. Previously degassed solvents were dried using an MBraun SPS-800 System (CH_2Cl_2, Et_2O and *n*-hexane) or over activated 3 Å molecular sieves (MeCN, ^{i}PrOH). Compounds $[NBu_4][(CF_3)_3Pt(CO)]$[S1] and $(CF_3)_3Au{\cdot}OEt_2$[S2] were prepared using published methods. All other reagents were purchased from standard commercial suppliers and used as received. Elemental analyses were carried out using a PerkinElmer 2400 CHNS/O Series II microanalyzer. IR spectra were recorded on neat solid samples using a PerkinElmer Spectrum FT-IR spectrometer (4000–250 cm^{-1}) equipped with an ATR device. NMR spectra were recorded on Bruker ARX 300 or AV 400 spectrometers. Unless otherwise stated, the spectroscopic measurements were carried out at room temperature. Chemical shifts of the measured nuclei (δ in ppm) are given with respect to the standard references in use: $SiMe_4$ (^{1}H and ^{13}C) and $CFCl_3$ (^{19}F). Where applicable, resonances were assigned by means of ^{1}H-^{1}H COSY, ^{1}H-^{13}C HSQC and ^{1}H-^{13}C HMBC experiments. The numbering scheme for the assignments of the signals corresponding to the quinoline ligands is given in Chart S1. Chemically inequivalent CF_3 groups are indicated as follows: CF_3–M–L refers to the CF_3 group *trans* to the neutral L ligand, whereas CF_3–M–CF_3 refers to the mutually *trans*-standing CF_3 groups. Multiplicity is indicated as follows: s = singlet, d = doublet, q = quartet, spt = septet, m = multiplet, m_c = multiplet centered at. NMR parameters associated with the $[NBu_4]^+$ cation in the Pt complexes are unexceptional and are therefore omitted.

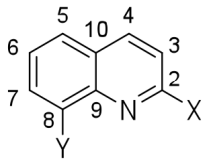

Chart S1. Numbering scheme for the ligands used in this work: 8-hydroxyquinoline (hq: X = H, Y = OH), 8-hydroxyquinaldine (hq': X = Me, Y = OH) and 8-methylquinoline (mq: X = H, Y = Me).

Synthesis of [NBu$_4$][(CF$_3$)$_3$Pt(NCMe)] (A) in solution: Me$_3$NO (12 mg, 149 μmol) was added to a solution of [NBu$_4$][(CF$_3$)$_3$Pt(CO)] (100 mg, 149 μmol) in 5 mL MeCN. After 2 h of stirring, the solution was concentrated to dryness. Addition of 5 mL CH_2Cl_2 gave a solution of complex **A**, which is suitable for most synthetic purposes. Full conversion was checked by ^{19}F NMR. **^{19}F NMR** (376.308 MHz, CD_3CN, 298 K; Figure S1): δ_F / ppm = −22.17 [spt, 3F, $^2J(^{195}Pt,F)$ = 940 Hz, $^4J(F,F)$ = 3.4 Hz; CF_3–Pt–L], −28.19 [q, 6F, $^2J(^{195}Pt, F)$ = 516 Hz; CF_3–Pt–CF_3].

Synthesis of [NBu$_4$][(CF$_3$)$_3$Pt(hq)] (1): The equimolar amount of hq (22 mg, 149 μmol) was added to a freshly-prepared solution of the precursor species **A** (149 μmol) in CH_2Cl_2 (5 mL). After 20 min of stirring, the solution was concentrated to dryness. By treating the resulting residue with *i*PrOH (2 mL), a yellow solid was formed, which was filtered, washed with *n*-hexane (3 mL), vacuum dried and identified as compound **1** (60 mg, 76 μmol, 51% yield). **IR** (Figure S16): $\tilde{\nu}$ / cm^{-1} = 2965 (m), 2938 (m), 2877 (w), 1617 (w), 1591 (w), 1580 (w), 1508 (m), 1499 (w), 1483 (m), 1463 (m), 1404 (w), 1387 (w), 1368 (w), 1337 (w), 1322 (w), 1286 (w), 1263 (m), 1215 (w), 1192 (w), 1173 (w), 1152 (s), 1135 (m), 1087 (vs), 1078 (vs), 1031 (s), 984 (vs), 899 (m), 880 (m), 831 (s), 800 (m), 783 (m), 768 (m), 752 (m), 740 (m), 730 (m), 692 (w), 632 (w), 590 (w), 542 (m), 522 (m), 510 (w), 477 (m), 454 (w), 408 (w), 375 (w), 348 (w), 321 (m), 314 (m), 287 (w), 278 (m), 270 (m). **^{1}H NMR** (300.130 MHz, CD_2Cl_2, 253 K; Figure S2): δ_H / ppm = 10.82 [s, 1H, $^1J(^{195}Pt,H)$ = 82.7 Hz; OH], 9.29 [dd, 1H, $^3J(^{195}Pt,H) \approx 25$ Hz, $^3J(H2,H3)$ = 5.0 Hz, $^4J(H2,H4)$ = 1.6 Hz; H2], 8.30 [dd, 1H, $^3J(H4, H3)$ = 8.4 Hz; H4], 7.53 (m_c, 1H; H6), 7.47–7.37 (m, 2H; H3 + H7), 7.28 [dd, 1H, $^3J(H5,H6)$ = 7.7 Hz $^4J(H5, H7)$ = 1.5 Hz; H5]. **^{13}C{^{1}H} NMR** (75.432 MHz, CD_2Cl_2, 253 K): δ_C / ppm = 151.6 (C2), 139.6 (C4), 128.5 (C6), 121.1/119.9 (C3/C7), 116.4 (C5).[S3] **^{19}F NMR** (282.231 MHz, CD_2Cl_2, 253 K; Figure S3): δ_F / ppm = −21.70 [spt, 3F, $^2J(^{195}Pt,F)$ = 858 Hz, $^4J(F,F)$ = 3.3 Hz; CF_3–Pt–L], −30.63 [q, 6F, $^2J(^{195}Pt,F)$ = 509 Hz; CF_3–Pt–CF_3]. **Elemental analysis** calcd (%) for $C_{28}H_{43}F_9N_2OPt$: C 42.6, H 5.5, N 3.55; found: C 42.2, H 5.1, N 3.3.

Synthesis of [NBu$_4$][(CF$_3$)$_3$Pt(hq')] (2): By using the procedure just described for the synthesis of **1**, compound **2** was prepared starting from a CH_2Cl_2 solution of the precursor species **A** (149 μmol) and hq' (24 mg, 149 μmol). Complex **2** was obtained as a white solid (65 mg, 81 μmol, 54% yield). **IR** (Figure S17): $\tilde{\nu}$ / cm^{-1} = 2963 (m), 2938 (m), 2876 (w), 1606 (w), 1569 (w), 1518 (w, sh), 1484 (m), 1457 (m), 1441 (m), 1425 (w), 1380 (w), 1358 (w), 1328 (w), 1319 (w), 1286 (w), 1260 (m), 1212 (w), 1196 (w), 1172 (w), 1151 (s), 1131 (m), 1107 (m), 1086 (vs), 1078 (vs), 1029 (s), 981 (vs), 959 (vs), 876 (m), 843 (s), 796 (w), 763 (m), 747 (m), 711 (w), 691 (w), 665 (w), 625 (w), 554 (m), 519 (w), 477 (w), 442 (w), 322 (m), 311 (m), 301 (m), 284 (w), 270 (m). **^{1}H NMR** (300.130 MHz, CD_2Cl_2, 253 K; Figure S4): δ_H / ppm = 11.10 [s, 1H, $^1J(^{195}Pt,H)$ = 100 Hz; OH], 8.16 [d, 1H, ^3J(H4,H3) = 8.4 Hz; H4], 7.45 (m$_c$, 1H; H6), 7.38–7.28 (m, 2H; H3 + H5), 7.24 (m$_c$, 1H; H7), 3.35 (s, 3H; CH_3). **^{13}C{^{1}H} NMR** (75.432 MHz, CD_2Cl_2, 253 K): δ_C / ppm = 162.3 (C2), 151.6 (C8), 139.8 (C4), 135.7 (C9), 129.8 (C10), 127.4 (C6), 123.8 (C3), 120.0 (C5), 117.3 (C7), 28.5 (CH_3). **^{19}F NMR** (282.231 MHz, CD_2Cl_2, 253 K; Figure S5): δ_F / ppm = −21.83 [spt, 3F, $^2J(^{195}Pt,F)$ = 867 Hz, ^4J(F,F) = 3.3 Hz; CF_3–Pt–L], −30.09 [q, 6F, $^2J(^{195}Pt,F)$ = 501 Hz; CF_3–Pt–CF_3]. **Elemental analysis** calcd (%) for $C_{29}H_{45}F_9N_2OPt$: C 43.3, H 5.6, N 3.5; found: C 43.0, H 5.5, N 3.5. **Single crystals** of **2** suitable for X-ray diffraction were obtained by slow diffusion of a layer of *n*-hexane (5 mL) into a solution of **2** (7 mg) in CH_2Cl_2 (2 mL) at –30 °C.

Synthesis of (CF$_3$)$_3$Au(hq) (3): The equimolar amount of hq (13 mg, 92 μmol) was added to a freshly-prepared solution of $(CF_3)_3Au{\cdot}OEt_2$ (92 μmol) in Et_2O/*n*-hexane (5/15 mL). The resulting mixture was stirred for 20 min. Removal of the solvent by vacuum evaporation afforded a white solid, which was suspended in *n*-hexane (2 mL), filtered, vacuum dried, and identified as compound **3** (36 mg, 66 μmol, 71% yield). **IR** (Figure S18): $\tilde{\nu}$ / cm^{-1} = 3581 (m, ν_{OH}), 1623 (w), 1593 (w), 1527 (m), 1477 (w), 1440 (w), 1420 (w), 1378 (m), 1324 (m), 1282 (w), 1262 (m), 1235 (w), 1205 (w), 1169 (s), 1144 (w), 1080 (vs), 1052 (vs), 972 (s), 954 (m), 914 (m), 886 (w), 824 (s), 802 (w), 777 (m), 756 (s), 740 (m), 730 (m), 711 (m), 593 (w), 580 (w), 538 (w), 522 (w), 499 (w), 478 (m), 444 (w), 338 (s), 329 (s), 314 (s), 303 (vs), 265 (s). **^{1}H NMR** (400.130

MHz, CD_2Cl_2, 298 K; Figure S6): δ_H / ppm = 8.97 [dd, 1H, ^3J(H2,H3) = 5.2 Hz, ^4J(H2,H4) = 1.4 Hz; H2), 8.57 [dd, 1H, ^3J(H4,H3) = 8.4 Hz; H4], 7.74 (dd, 1H; H3), 7.69–7.62 (m, 2H; H5 + H6), 7.40 (m_c, 1H; H7), 7.03 (br s, 1H; OH). **$^{13}C\{^1H\}$ NMR** (100.577 MHz, CD_2Cl_2, 298 K): δ_C / ppm = 151.1 (C2), 148.0 (C8), 142.7 (C4), 135.5 (C9), 132.3 (C10), 129.7/122.9 (C5/C6), 122.7 (C3), 117.6 (C7). **^{19}F NMR** (376.308 MHz, CD_2Cl_2, 298 K; Figure S7): δ_F / ppm = −27.96 [spt, 3F, ^4J(F,F) = 6.2 Hz; CF_3–Au–L], −38.20 (q, 6F; CF_3–Au–CF_3). **Elemental analysis** calcd (%) for $C_{12}H_7AuF_9NO$: C 26.25, H 1.3, N 2.55; found: C 26.3, H 1.3, N 2.6.

Single crystals of **3**·OEt_2 suitable for X-ray diffraction were obtained after cooling a solution of **3** (7 mg) in Et_2O/*n*-hexane (2/4 mL) at −30 °C for several days.

Single crystals of **3**·OH_2 suitable for X-ray diffraction were obtained by slow diffusion of a layer of *n*-hexane (5 mL) into a solution of **3** (7 mg) in wet CH_2Cl_2 (2 mL) at −30 °C. Preferential crystallization of the hydrate occurs. Many other attempts using thoroughly dried solvents produced just poor-quality crystals of no use for XRD purposes.

Synthesis of $(CF_3)_3Au$(hq') (4): By using the procedure just described for the synthesis of **3**, compound **4** was prepared starting from a Et_2O/*n*-hexane solution of $(CF_3)_3Au{\cdot}OEt_2$ (92 μmol) and hq' (15 mg, 92 μmol). Complex **4** was isolated as a white solid (38 mg, 67 μmol, 73% yield). **IR** (Figure S19): $\tilde{\nu}$ / cm^{-1} = 3575 (m, ν_{OH}), 1623 (w), 1606 (w), 1581 (m), 1524 (m), 1481 (w), 1440 (m), 1388 (w), 1374 (w), 1353 (m), 1334 (w), 1327 (w), 1298 (w), 1281 (w), 1266 (w), 1222 (m), 1202 (w), 1168 (s), 1150 (w), 1082 (vs), 1058 (vs), 986 (s), 966 (s), 927 (m), 881 (m), 835 (s), 754 (s), 729 (m), 711 (m), 657 (m), 580 (w), 570 (w), 540 (w), 529 (w), 511 (m), 452 (w), 441 (w), 416 (w), 325 (s), 315 (s), 297 (vs), 260 (s). **^1H NMR** (400.130 MHz, CD_2Cl_2, 298 K; Figure S9): δ_H / ppm = 8.42 [d, 1H, ^3J(H4,H3) = 8.5 Hz; H4], 7.64–7.55 (m, 3H; H3 + H5 + H6), 7.36 [dd, 1H, ^3J(H7,H6) = 7.0 Hz, ^4J(H7,H5) = 2.0 Hz; H7], 6.66 (br s, 1H; OH), 3.22 (s, 3H; CH_3). **$^{13}C\{^1H\}$ NMR** (100.577 MHz, CD_2Cl_2, 298 K): δ_C / ppm = 161.3 (C2), 147.6 (C8), 142.3 (C4), 135.2 (C9), 130.4 (C10), 128.6 (C6), 125.4 (C3), 122.8 (C5), 117.9 (C7), 27.6 (CH_3). **^{19}F NMR** (376.308 MHz, CD_2Cl_2, 298 K; Figure S10):

δ_F / ppm = −28.50 [spt, 3F, ^4J(F,F) = 6.0 Hz, CF_3–Au–L], −37.53 (q, 6F; CF_3–Au–CF_3). **Elemental analysis** calcd (%) for $C_{13}H_9AuF_9NO$: C 27.7, H 1.6, N 2.5; found: C 27.85, H 1.7, N 2.5.

Synthesis of [NBu_4][$(CF_3)_3$Pt(mq)] (5): Me_3NO (12 mg, 149 μmol) was added to a solution of [NBu_4][$(CF_3)_3$Pt(CO)] (100 mg, 149 μmol) and mq (63 μL, 446 μmol) in 5 mL CH_2Cl_2. After 2 h of stirring, the solution was concentrated to dryness. By treating the resulting residue with *i*PrOH (2 mL), a yellow solid was formed, which was filtered, washed with *n*-hexane (3 mL), vacuum dried and identified as compound **5** (64 mg, 81 μmol, 55% yield). **IR** (Figure S20): $\tilde{\nu}$ / cm^{-1} = 2967 (m), 2937 (w), 2878 (w), 2117 (w), 1599 (w), 1509 (m), 1484 (m), 1465 (m), 1448 (w), 1421 (w), 1383 (w), 1356 (w), 1304 (w), 1198 (w), 1147 (s), 1130 (w), 1097 (m), 1069 (vs), 1014 (s), 970 (vs), 957 (vs), 938 (s), 880 (m), 828 (s), 804 (m), 783 (s), 771 (m), 740 (m), 731 (m), 722 (m), 688 (w), 578 (w), 550 (w), 525 (w), 490 (w), 477 (w), 464 (w), 440 (w), 314 (s), 298 (m), 283 (w), 269 (m). **^{1}H NMR** (400.130 MHz, CD_2Cl_2, 273 K; Figure S12): δ_H / ppm = 9.67 [dd, sh, 1H, ^3J(H2,H3) = 5.1 Hz, ^4J(H2,H4) = 1.6 Hz; H2], 8.28 [dd, 1H, ^3J(H4,H3) = 8.2 Hz; H4], 7.74 [br d, 1H, ^3J(H5,H6) = 8.0 Hz; H5], 7.66 [br d, 1H, ^3J(H7,H6) = 7.0 Hz; H7], 7.49 (m_c, 1H; H6), 7.40 (dd, 1H; H3), 3.83 (s, 3H; CH_3). **^{13}C{^{1}H} NMR** (100.577 MHz, CD_2Cl_2, 273 K): δ_C / ppm = 154.5 (C2), 145.0 (C9), 139.5 (C4), 134.2 (C7), 127.8 (C5), 127.1 (C6), 120.5 (C3), 22.7 (CH_3).[S4] **^{19}F NMR** (282.231 MHz, CD_2Cl_2, 273 K; Figure S13): δ_F / ppm = −18.66 [spt, 3F, ^2J(^{195}Pt,F) = 908 Hz, ^4J(F,F) = 3.2 Hz; CF_3–Pt–L], −28.92 [q, 6F, ^2J(^{195}Pt,F) = 516 Hz; CF_3–Pt–CF_3]. **Elemental analysis** calcd (%) for $C_{29}H_{45}F_9N_2Pt$: C 44.2, H 5.8, N 3.6; found: C 43.8, H 5.4, N 3.3. **Single crystals** of **5** suitable for X-ray diffraction were obtained by slow diffusion of a layer of *n*-hexane (5 mL) into a solution of **5** (7 mg) in CH_2Cl_2 (2 mL) at −30 °C.

Synthesis of $(CF_3)_3$Au(mq) (6): By using the procedure just described for the synthesis of **3**, compound **6** was prepared starting from an Et_2O/*n*-hexane solution of compound $(CF_3)_3Au{\cdot}OEt_2$ (92 μmol) and mq (13 μL, 92 μmol). Complex **6** was obtained as a white solid (34 mg, 62 μmol, 68% yield). **IR** (Figure S21): $\tilde{\nu}$ / cm^{-1} =

1612 (w), 1598 (w), 1516 (m), 1474 (w), 1460 (w), 1452 (w), 1396 (w), 1378 (w), 1361 (w), 1310 (w), 1166 (m), 1098 (vs), 1085 (vs), 1064 (vs), 1042 (vs), 1025 (vs), 991 (s), 981 (s), 957 (m), 914 (m), 891 (m), 825 (s), 804 (w), 773 (s), 763 (m), 732 (m), 725 (m), 711 (m), 626 (w), 579 (w), 545 (m), 532 (w), 525 (m), 489 (m), 468 (m), 462 (m), 433 (m), 311 (m), 303 (s). **^{1}H NMR** (400.130 MHz, CD_2Cl_2, 298 K; Figure S14): δ_H / ppm = 9.06 [dd, 1H, ^{3}J(H2,H3) = 5.3 Hz, ^{4}J(H2,H4) = 1.5 Hz; H2], 8.62 [dd, 1H, ^{3}J(H4,H3) = 8.2 Hz; H4], 7.95 [br d, 1H, ^{3}J(H5,H6) = 8.1 Hz; H5], 7.88 (m_c, 1H; H7), 7.75 (dd, 1H; H3), 7.70 (m_c, 1H; H6), 3.44 (s, 3H; CH_3). **^{13}C{^{1}H} NMR** (100.577 MHz, CD_2Cl_2, 298 K): δ_C / ppm = 151.8 (C2), 144.7 (C9), 144.2 (C4), 137.3 (C7), 132.2 (C10), 131.9 (C8), 129.4/129.3 (C5/C6), 121.9 (C3), 20.5 (CH_3). **^{19}F NMR** (376.308 MHz, CD_2Cl_2, 298 K; Figure S15): δ_F / ppm = −27.85 [spt, 3F, ^{4}J(F,F) = 6.4 Hz; CF_3–Au–L], −37.58 (q, 6F; CF_3–Au–CF_3). **Elemental analysis** calcd (%) for $C_{13}H_9AuF_9N$: C 28.5, H 1.7, N 2.6; found: C 28.85, H 1.7, N 2.7. **Single crystals** of **6** suitable for X-ray diffraction were obtained by slow diffusion of a layer of *n*-hexane (5 mL) into a solution of **6** (7 mg) in CH_2Cl_2 (2 mL) at 4 °C.

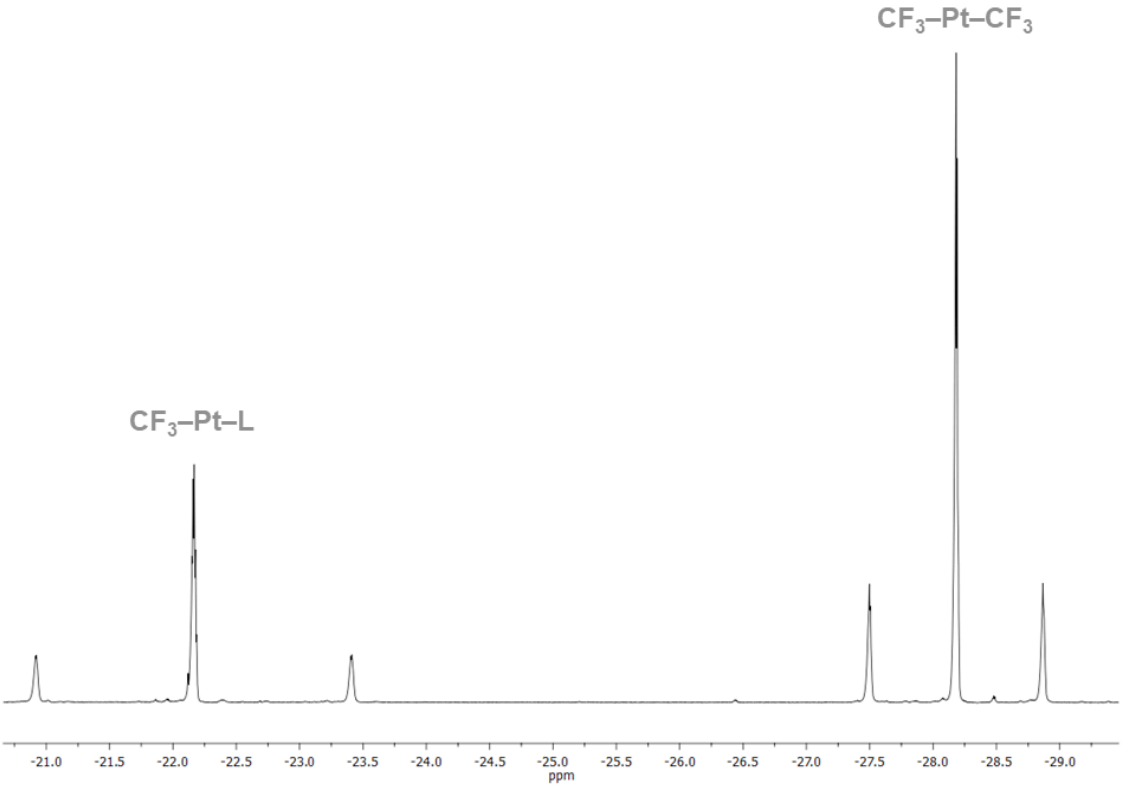

Figure S1. ^{19}F NMR spectrum (376.308 MHz) of $[NBu_4][(CF_3)_3Pt(NCMe)]$ (**A**) in CD_3CN solution at 298 K.

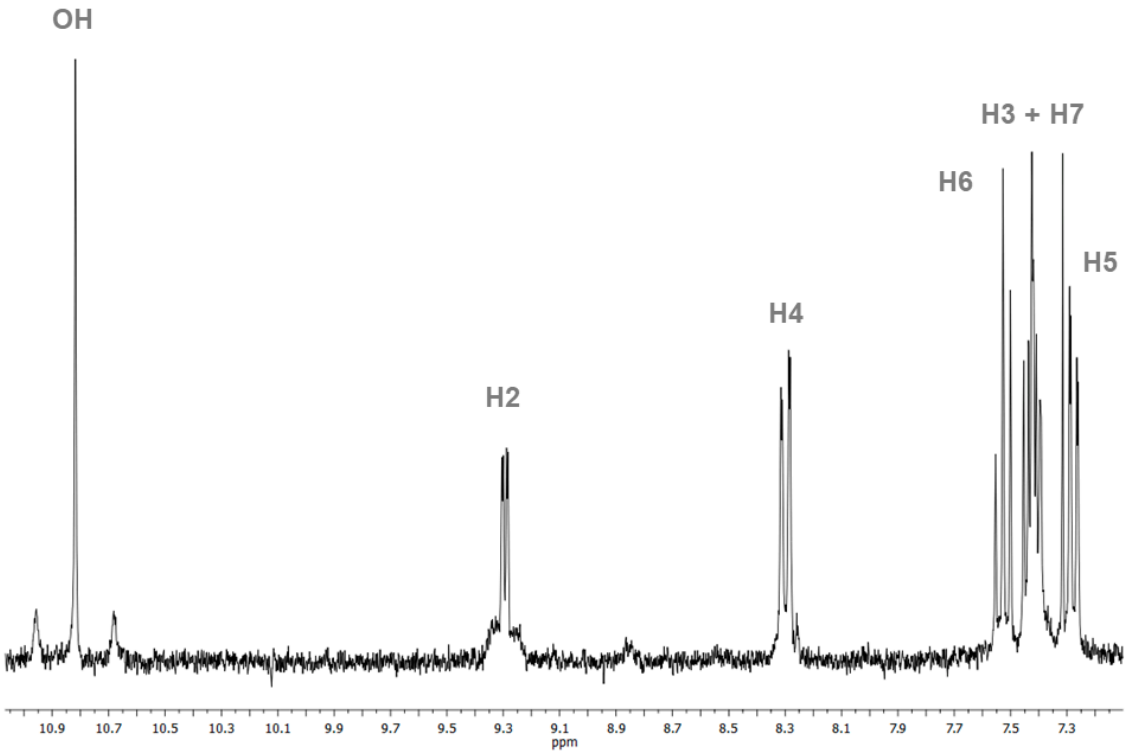

Figure S2. ^{1}H NMR spectrum (300.130 MHz) of [NBu_4][$(CF_3)_3Pt(hq)$] (**1**) in CD_2Cl_2 solution at 253 K.

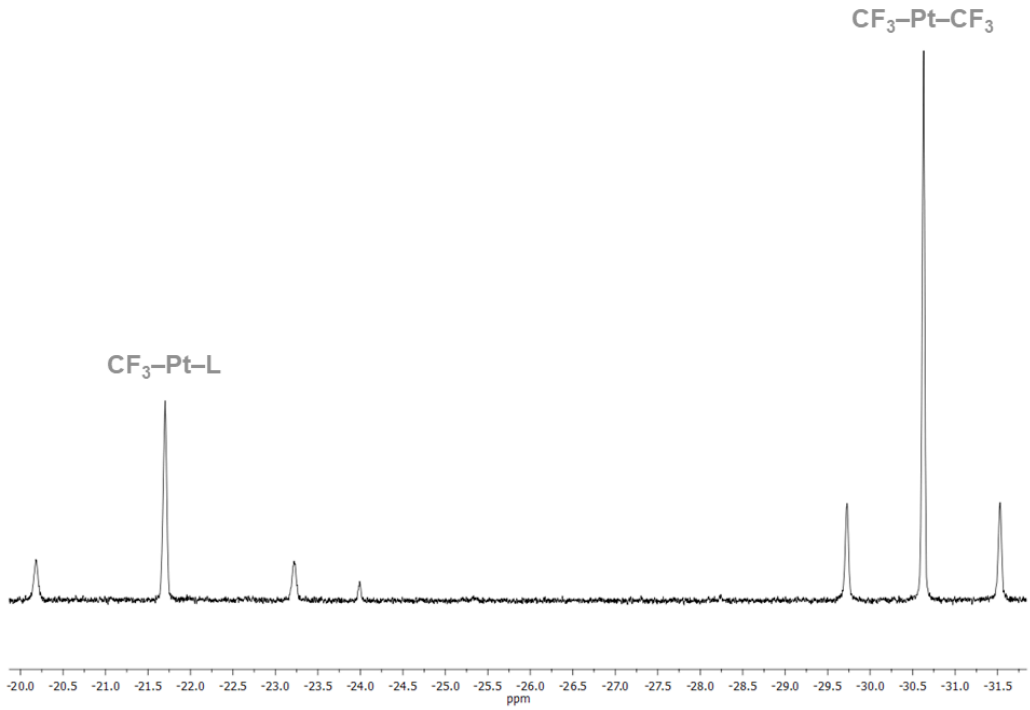

Figure S3. ^{19}F NMR spectrum (282.231 MHz) of [NBu_4][$(CF_3)_3Pt(hq)$] (**1**) in CD_2Cl_2 solution at 253 K.

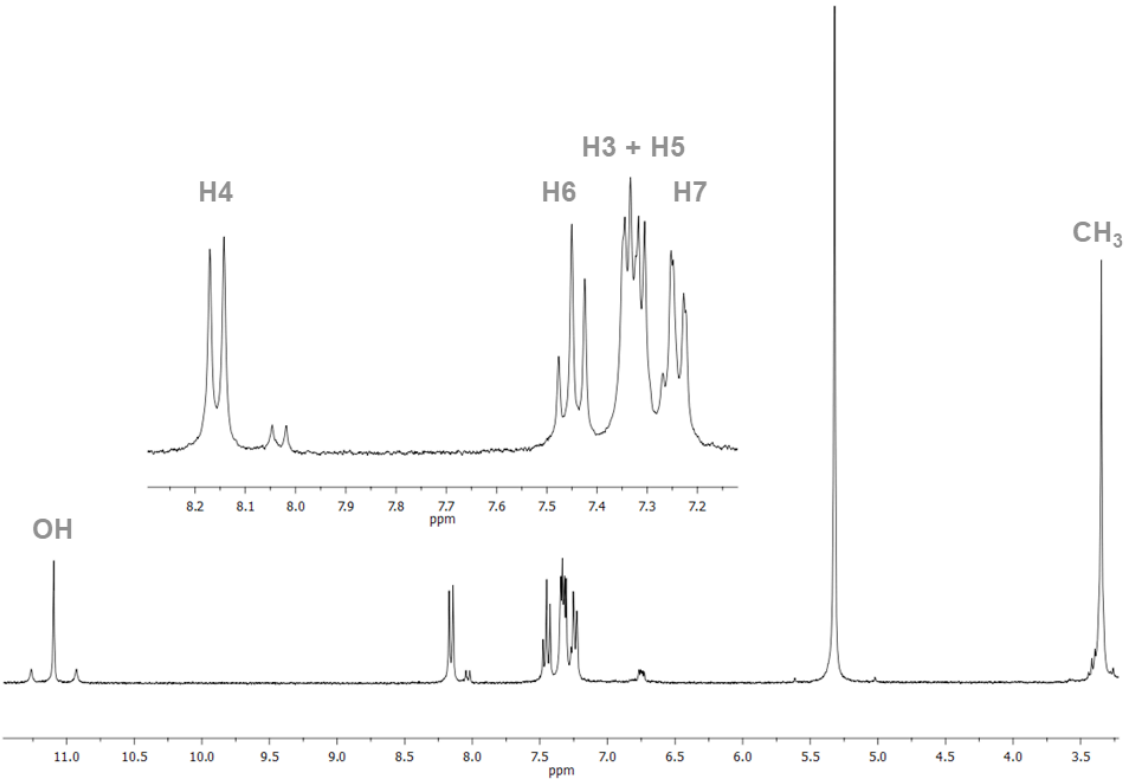

Figure S4. ^{1}H NMR spectrum (300.130 MHz) of [NBu_4][$(CF_3)_3$Pt(hq')] (**2**) in CD_2Cl_2 solution at 253 K (*cf*. Figure 1b).

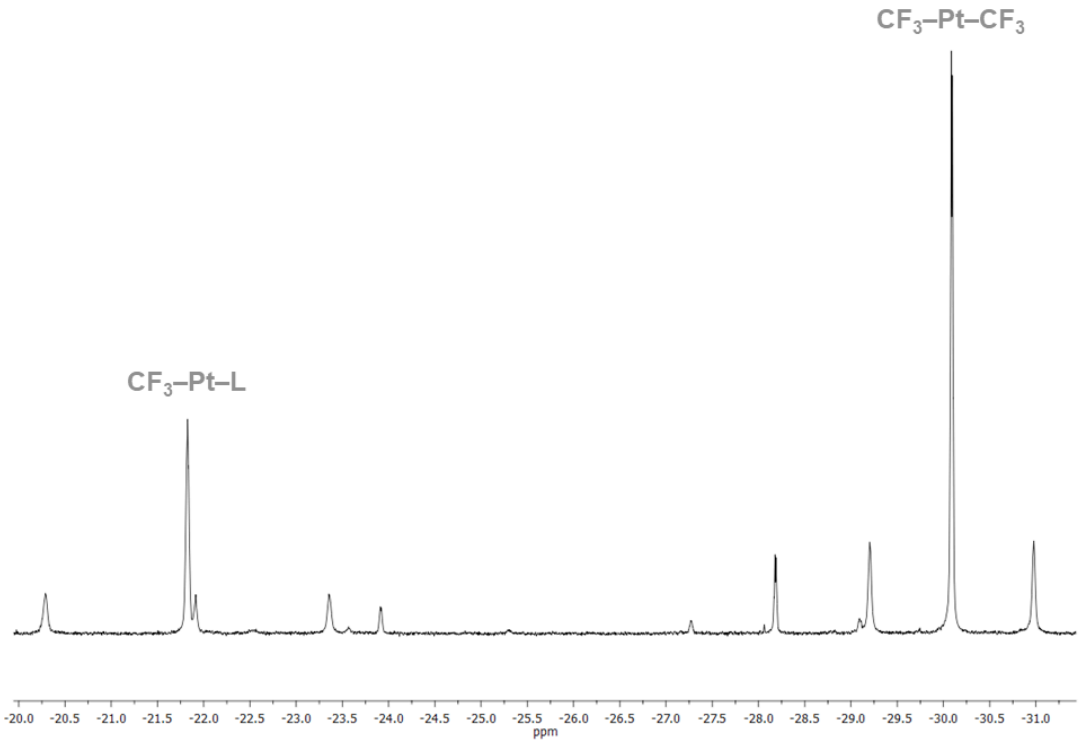

Figure S5. ^{19}F NMR spectrum (282.231 MHz) of [NBu_4][$(CF_3)_3$Pt(hq')] (**2**) in CD_2Cl_2 solution at 253 K.

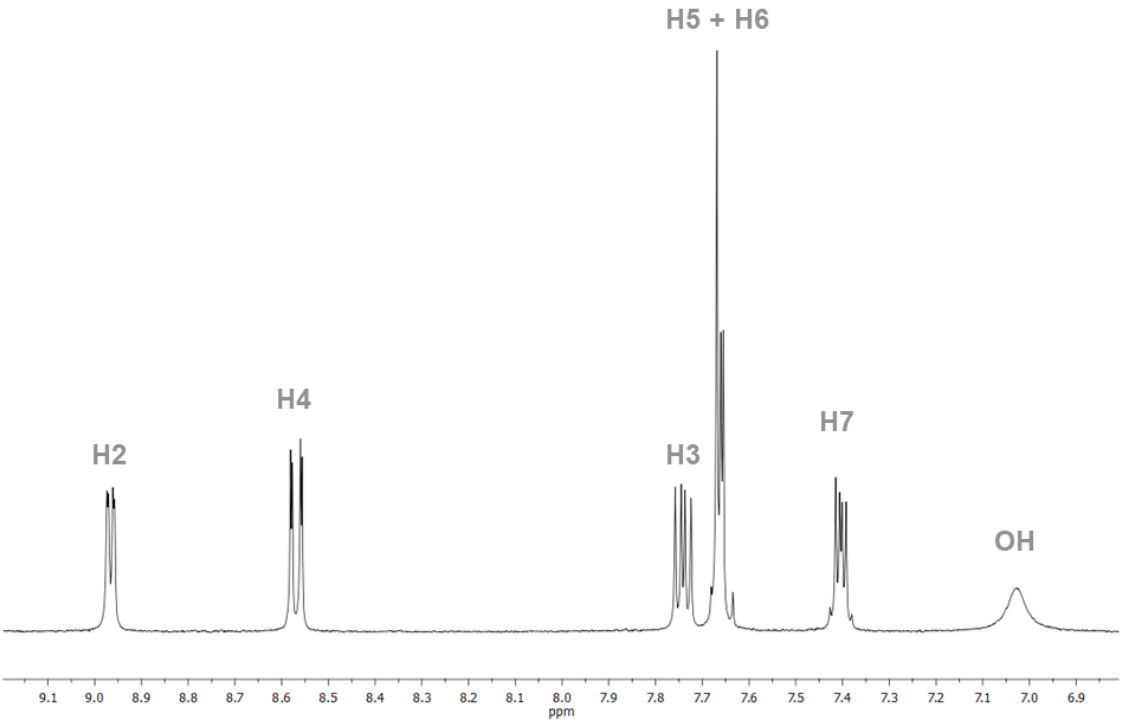

Figure S6. ^{1}H NMR spectrum (400.130 MHz) of $(CF_3)_3Au(hq)$ (**3**) in CD_2Cl_2 solution at 298 K.

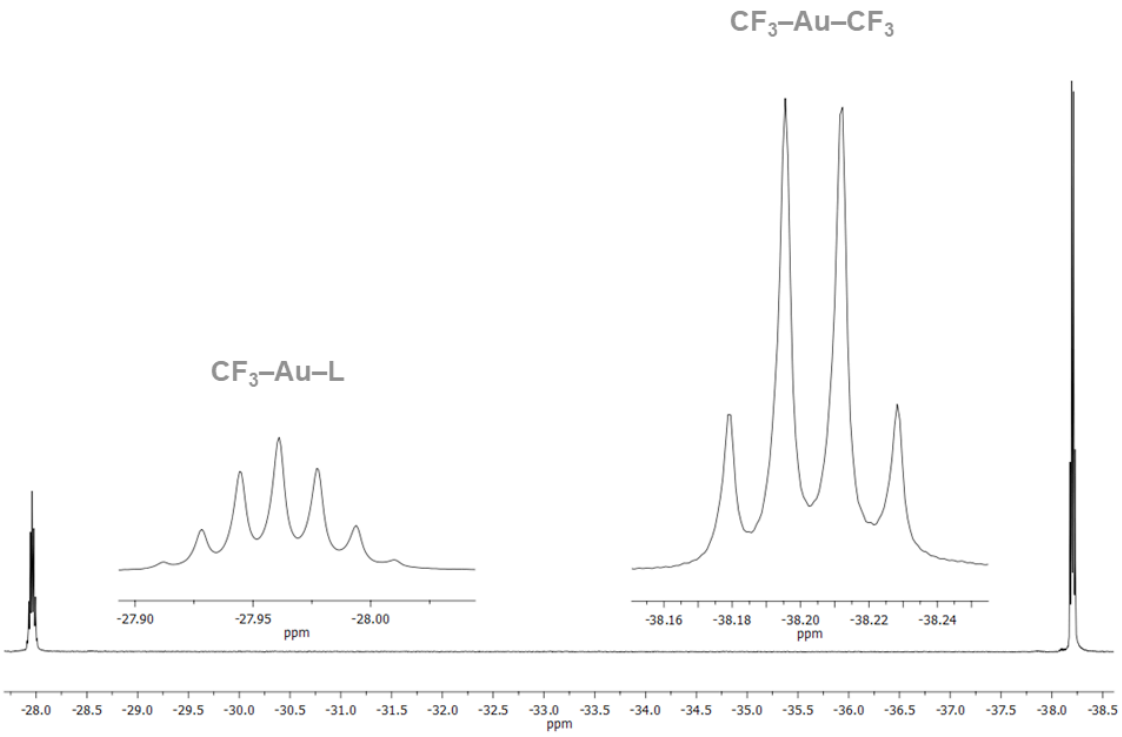

Figure S7. ^{19}F NMR spectrum (376.308 MHz) of $(CF_3)_3Au(hq)$ (**3**) in CD_2Cl_2 solution at 298 K.

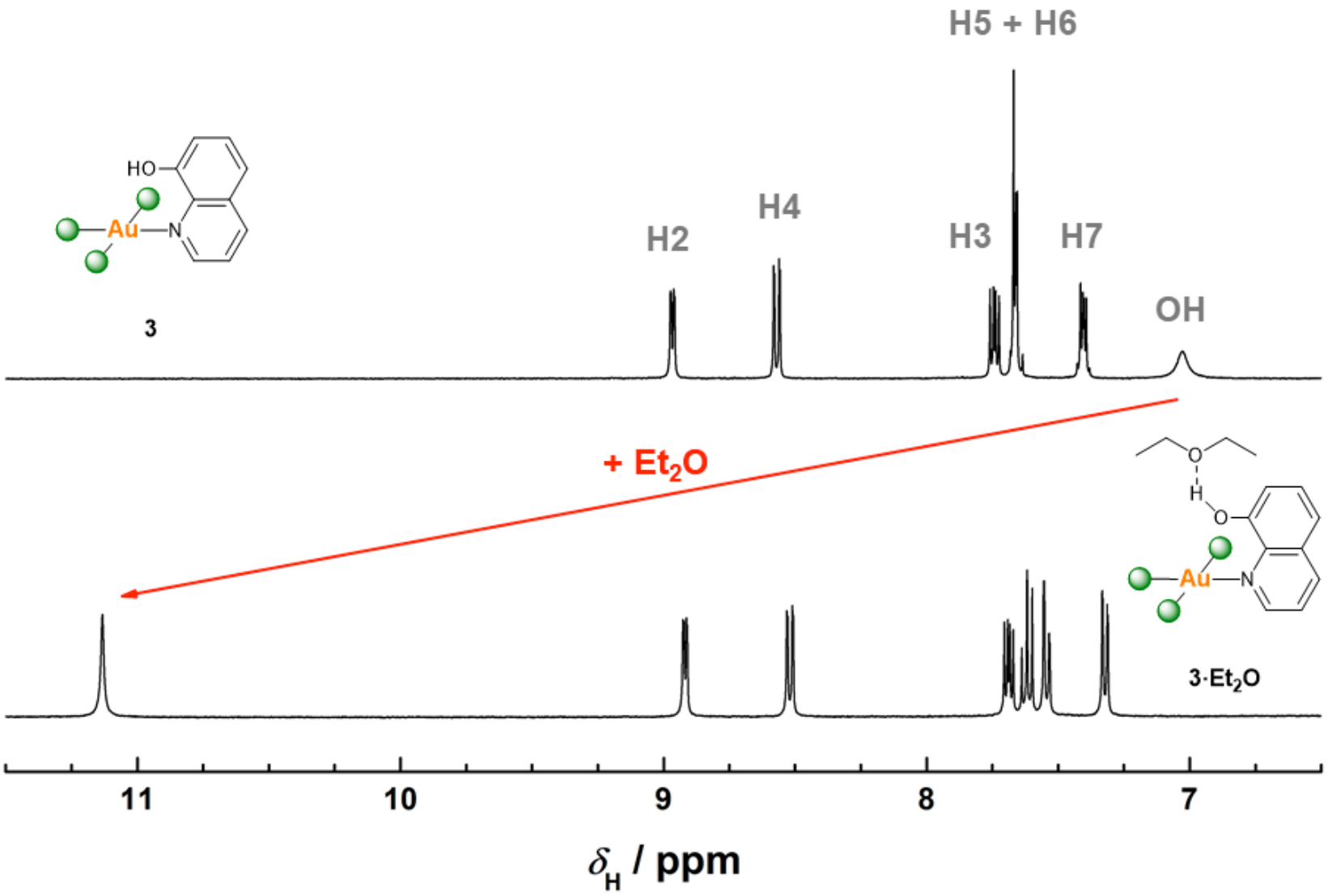

Figure S8. Low-field region of the ^{1}H NMR spectrum (400.130 MHz) of $(CF_3)_3Au(hq)$ (**3**) in CD_2Cl_2 solution at room temperature (above) and upon addition of Et_2O to the sample (below). The dramatic downfield shift observed in the resonance of the OH unit is in line with the formation of the **3**·OEt_2 adduct (see Figure 2a).

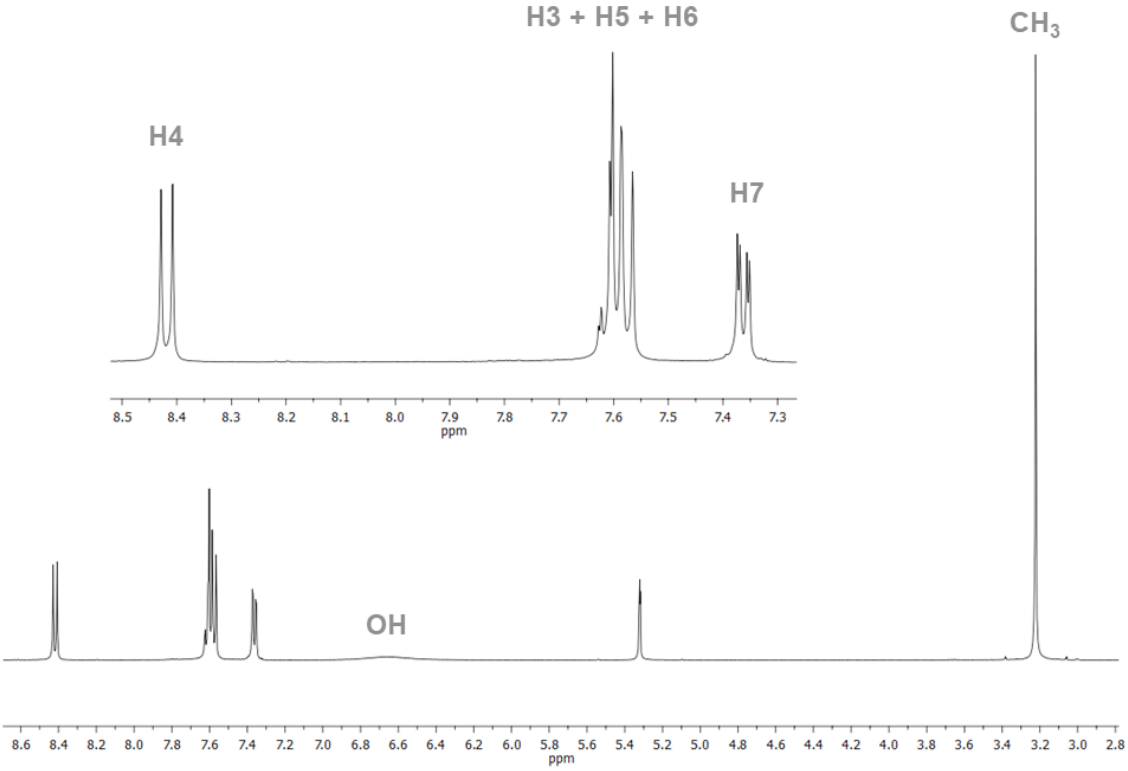

Figure S9. ^{1}H NMR spectrum (400.130 MHz) of $(CF_3)_3Au(hq')$ (**4**) in CD_2Cl_2 solution at 298 K.

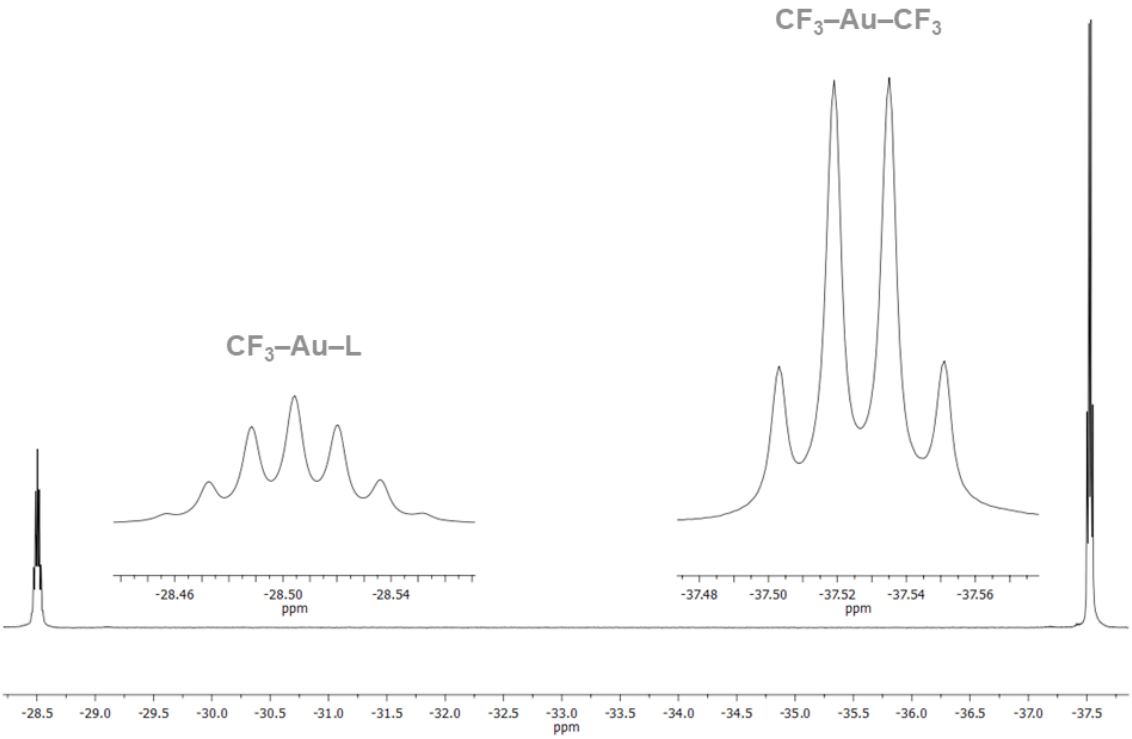

Figure S10. ^{19}F NMR spectrum (376.308 MHz) of $(CF_3)_3Au(hq')$ (**4**) in CD_2Cl_2 solution at 298 K.

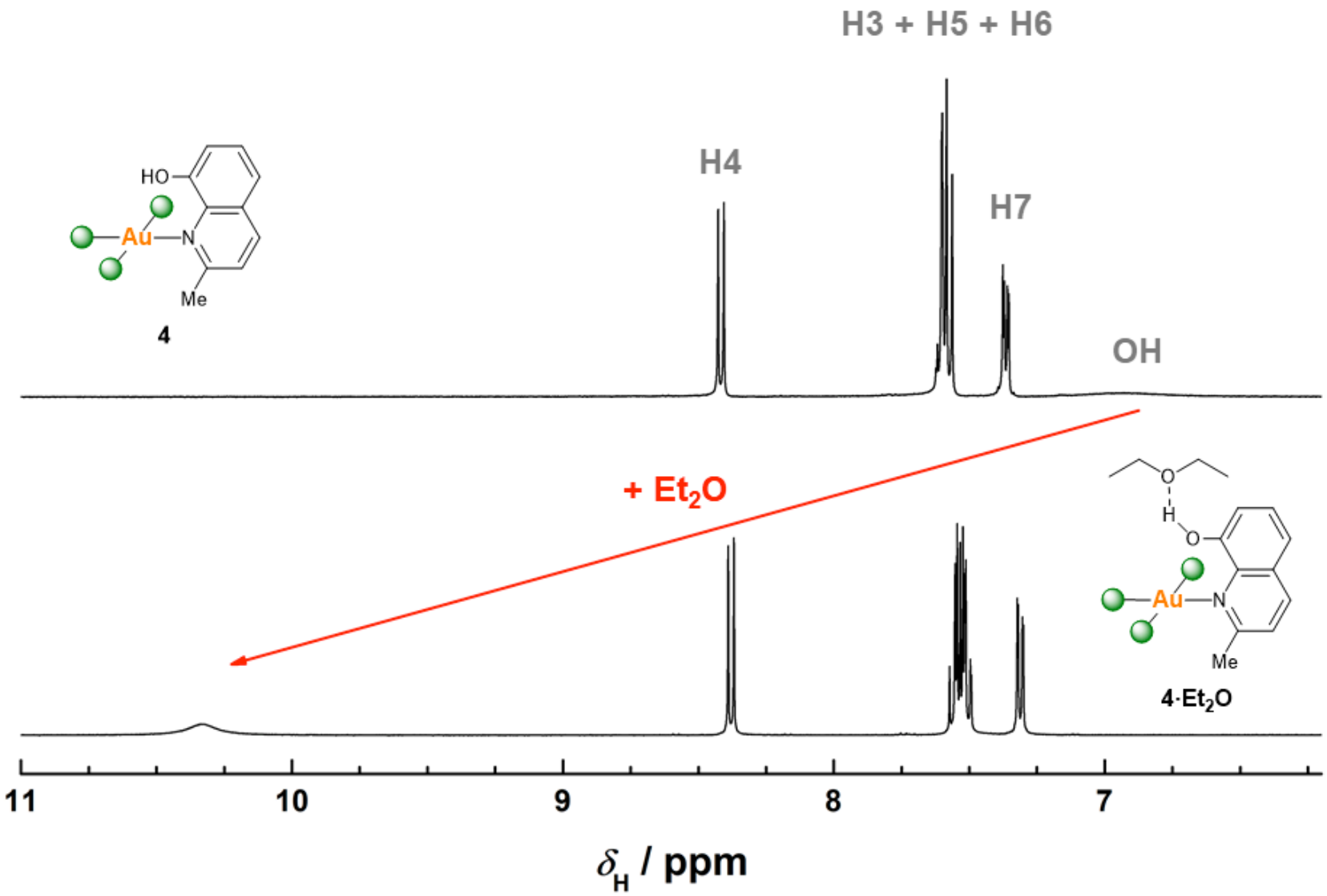

Figure S11. Low-field region of the ^{1}H NMR spectrum (400.130 MHz) of $(CF_3)_3Au(hq')$ (**4**) in CD_2Cl_2 solution at room temperature (above) and upon addition of Et_2O to the sample (below). The dramatic downfield shift observed in the resonance of the OH unit is in line with the formation of the **4**·OEt_2 adduct.

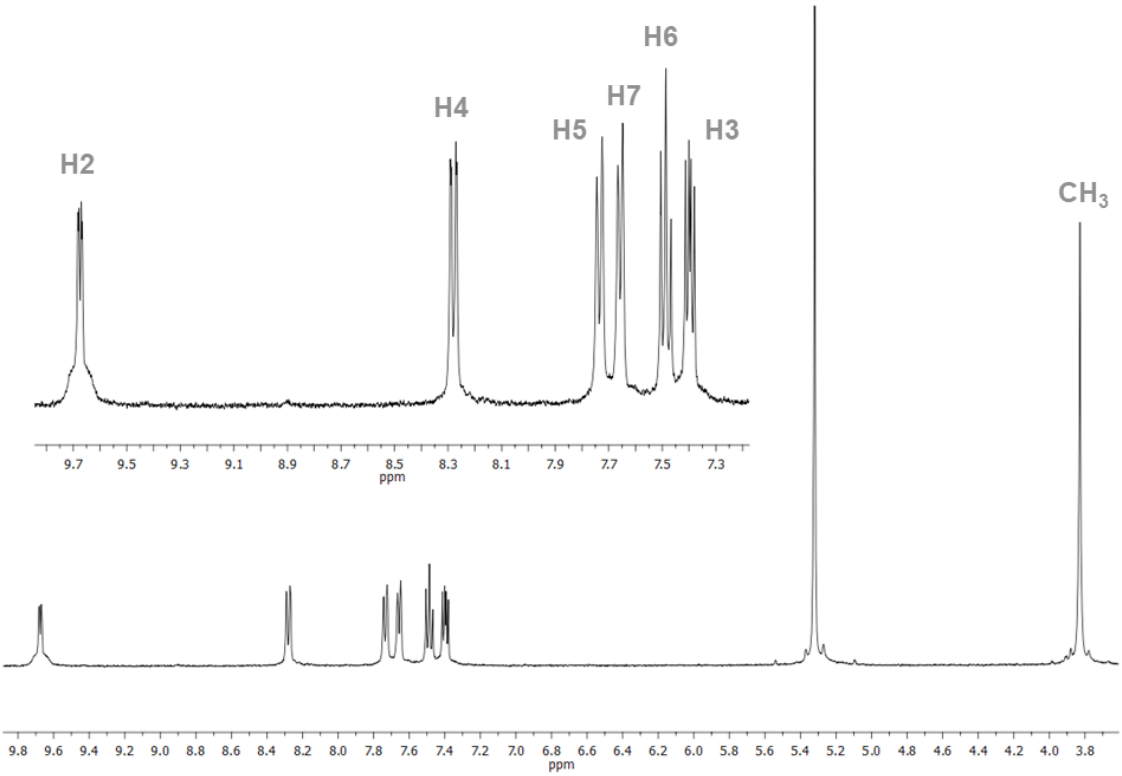

Figure S12. ^{1}H NMR spectrum (400.130 MHz) of [NBu_4][$(CF_3)_3Pt(mq)$] (**5**) in CD_2Cl_2 solution at 273 K.

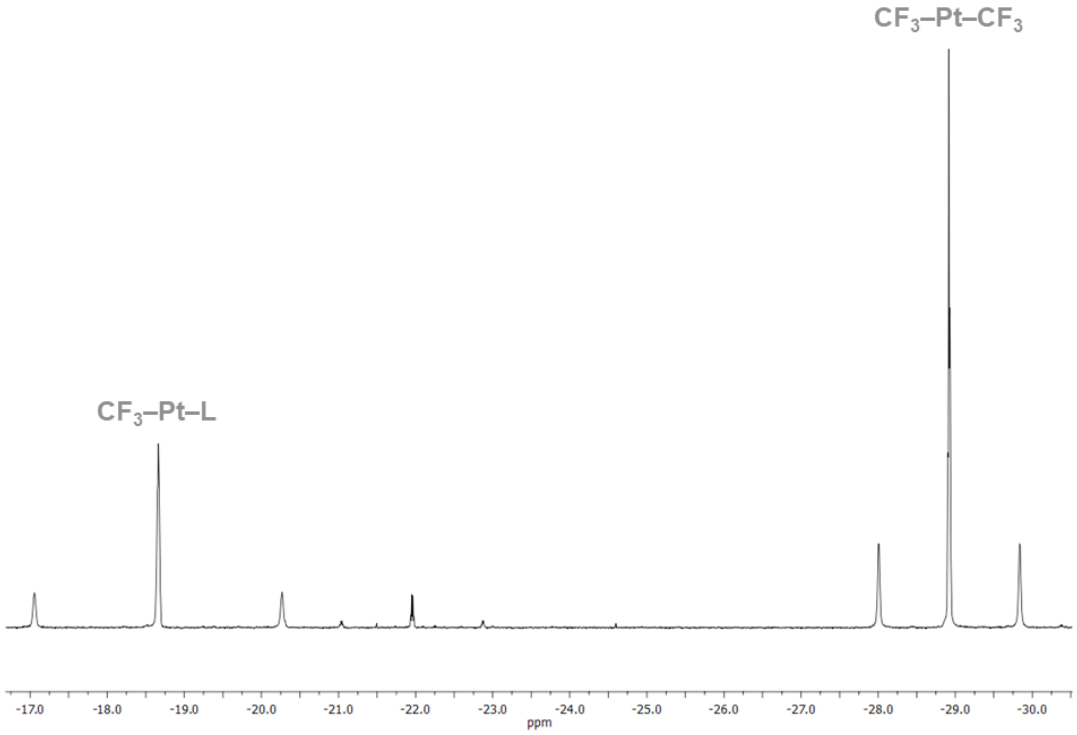

Figure S13. ^{19}F NMR spectrum (282.231 MHz) of [NBu_4][$(CF_3)_3Pt(mq)$] (**5**) in CD_2Cl_2 solution at 273 K.

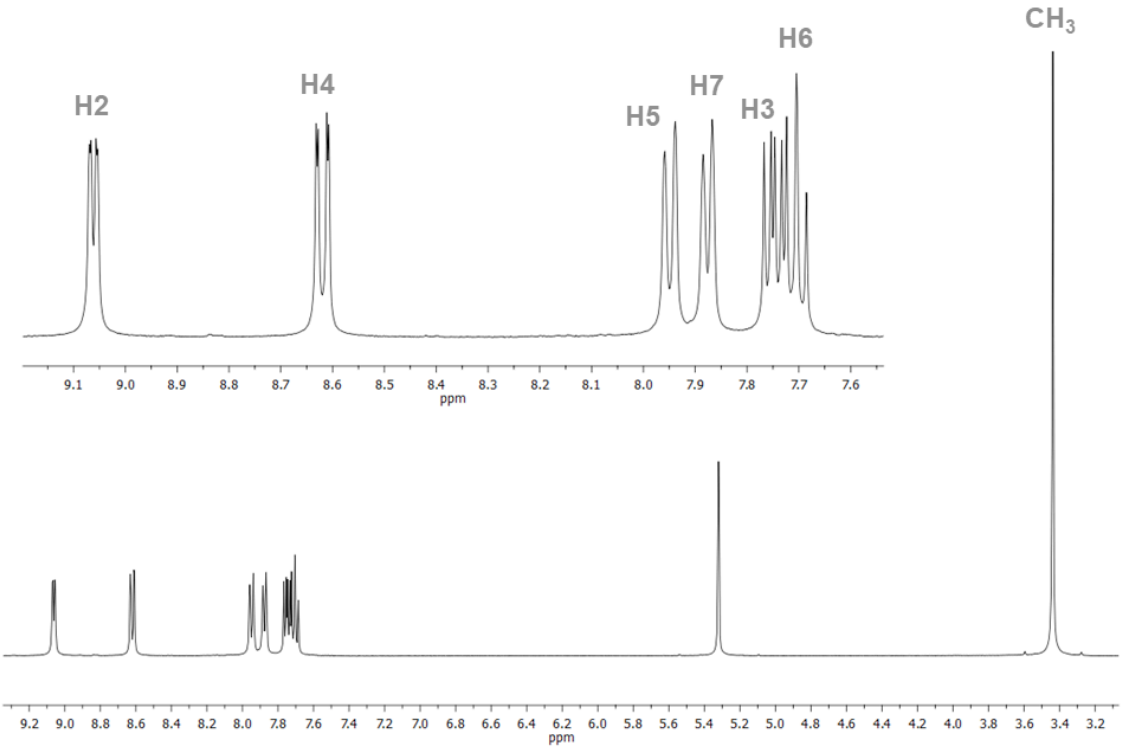

Figure S14. ^{1}H NMR spectrum (400.130 MHz) of $(CF_3)_3Au(mq)$ (**6**) in CD_2Cl_2 solution at 298 K.

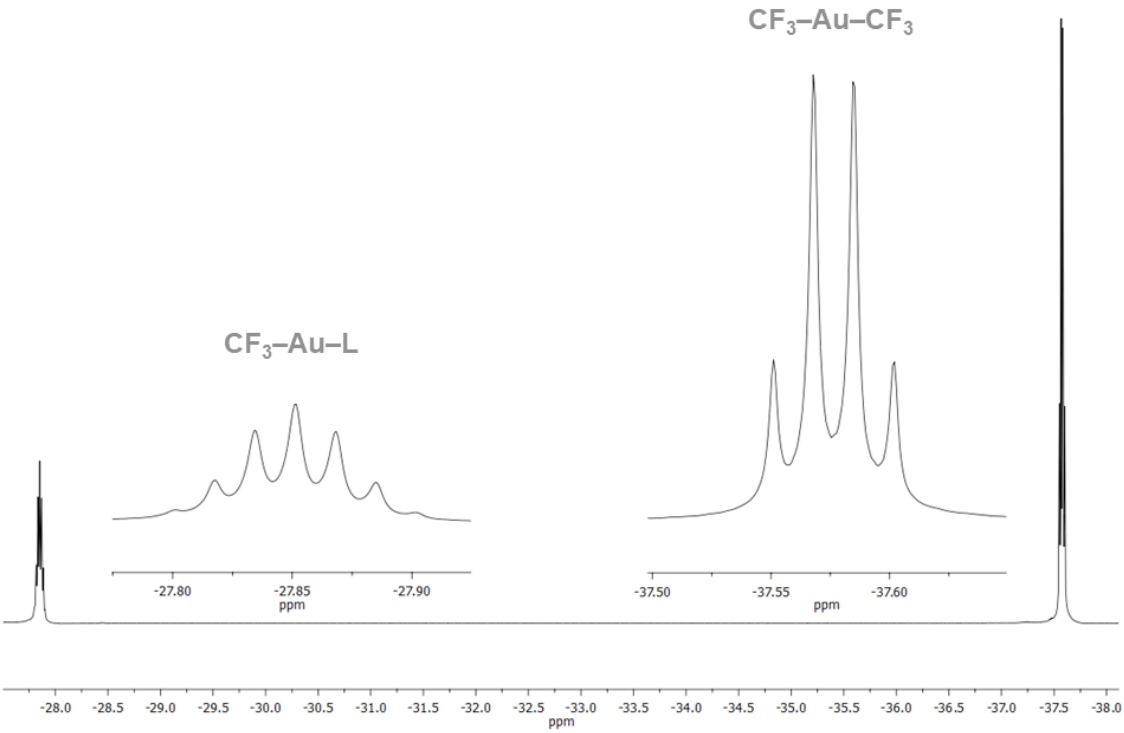

Figure S15. ^{19}F NMR spectrum (376.308 MHz) of $(CF_3)_3Au(mq)$ (**6**) in CD_2Cl_2 solution at 298 K.

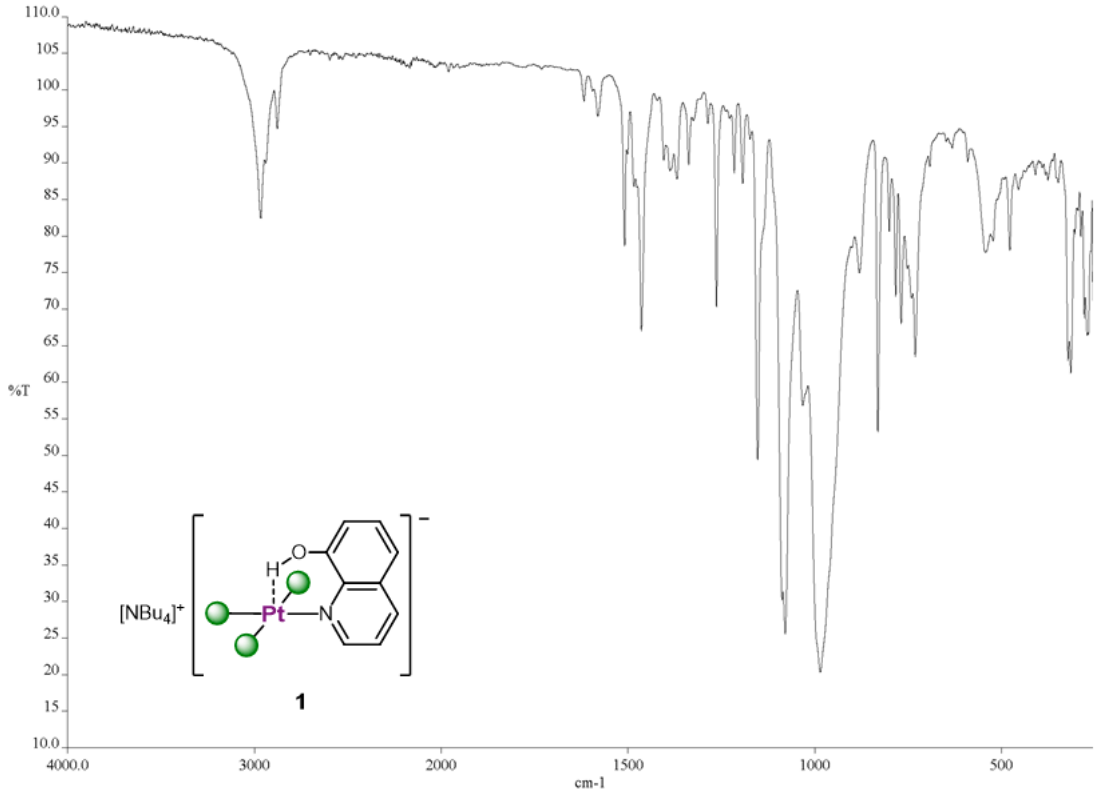

Figure S16. IR spectrum of compound **1**. No absorption above 3000 cm^{-1} is observed.

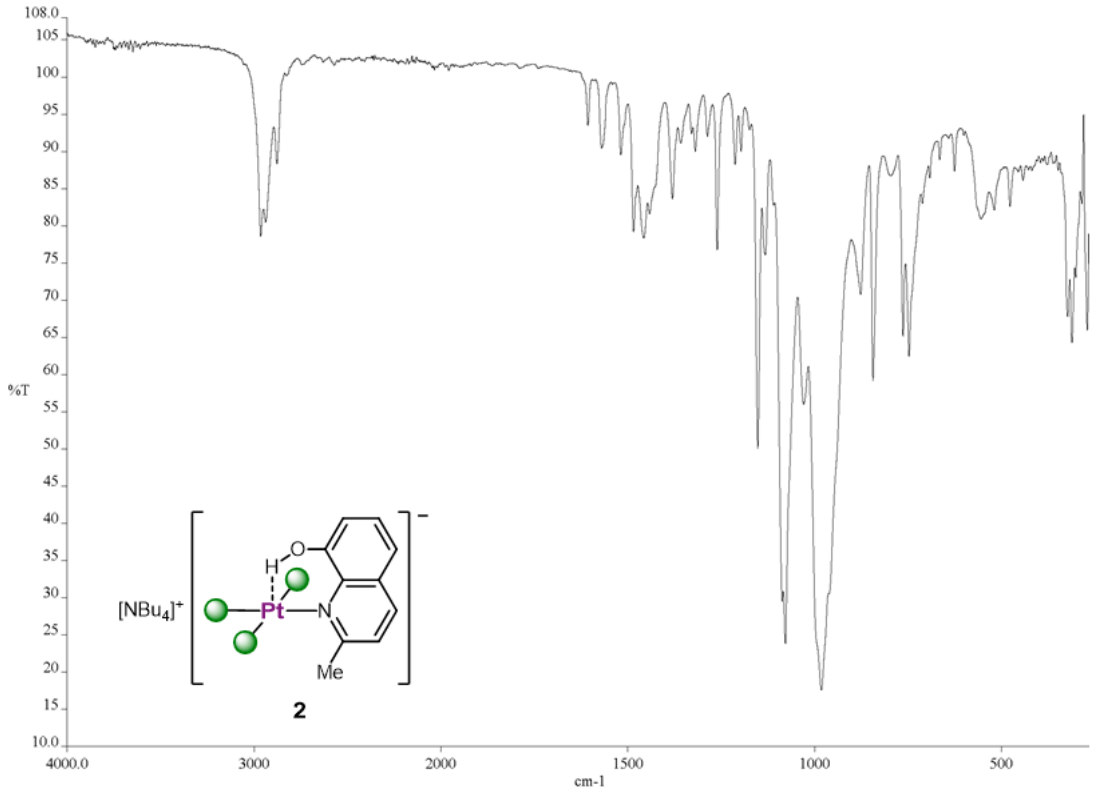

Figure S17. IR spectrum of compound **2**. No absorption above 3000 cm^{-1} is observed.

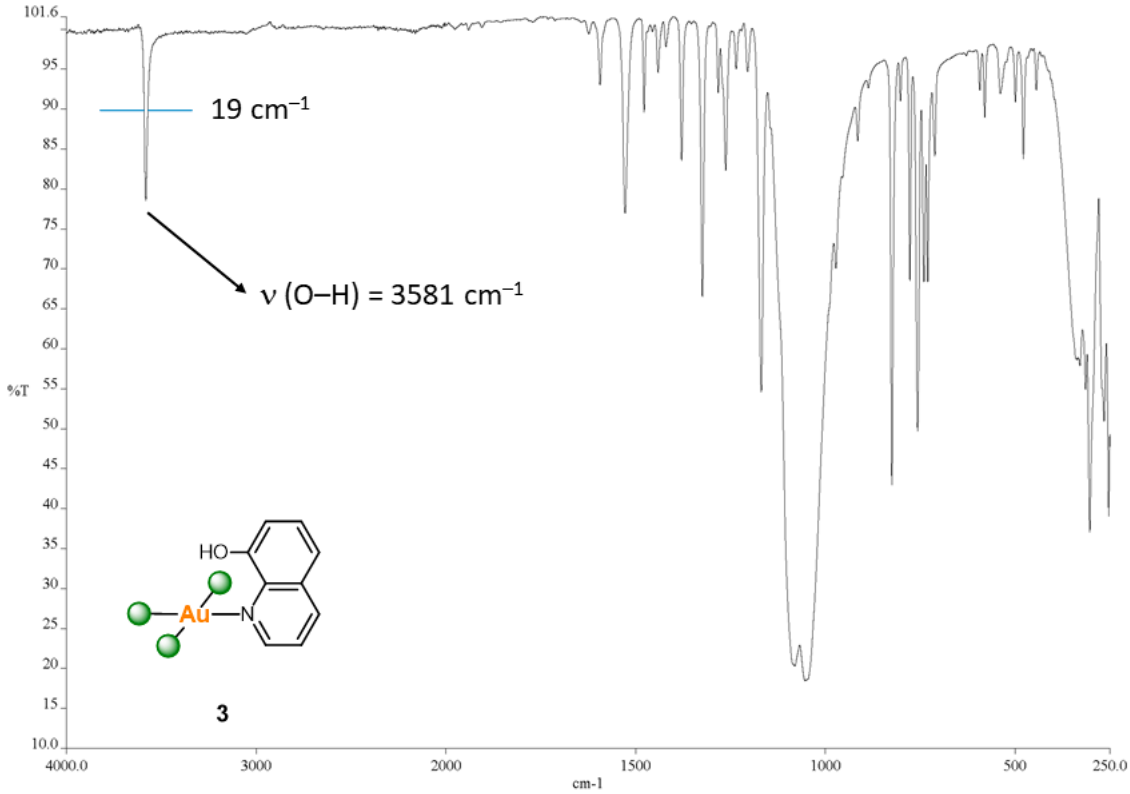

Figure S18. IR spectrum of compound **3**.

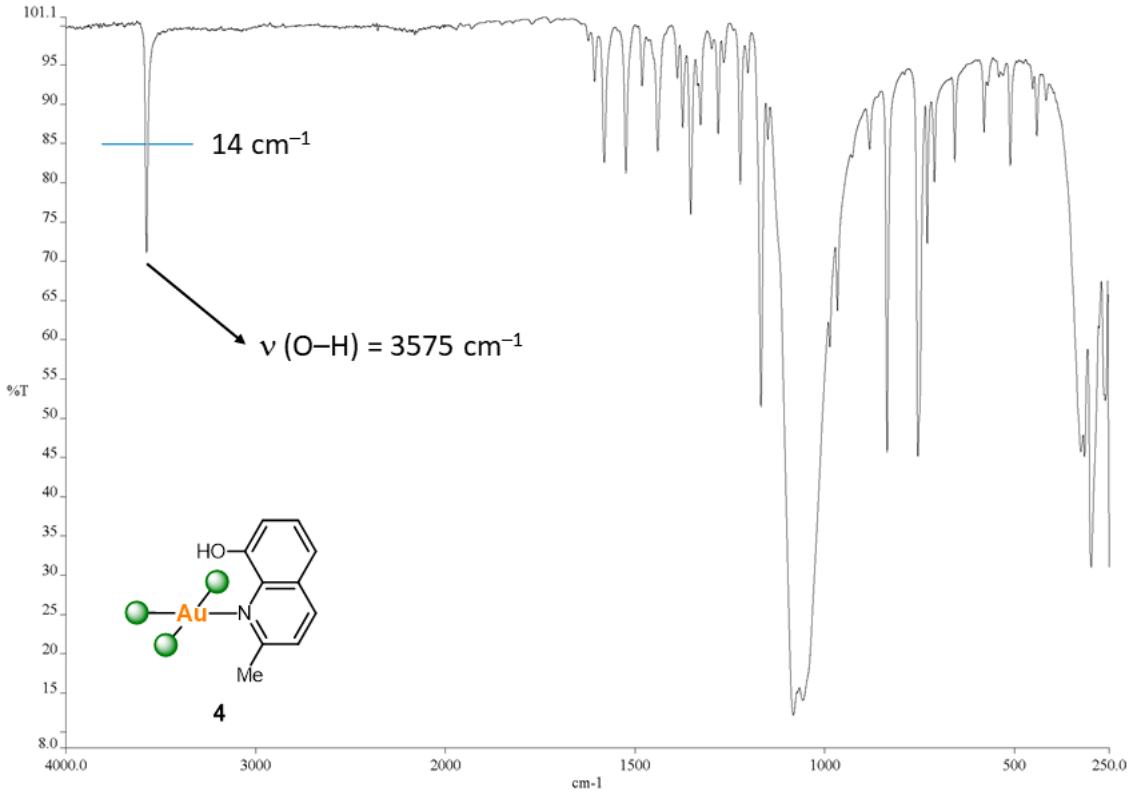

Figure S19. IR spectrum of compound **4**.

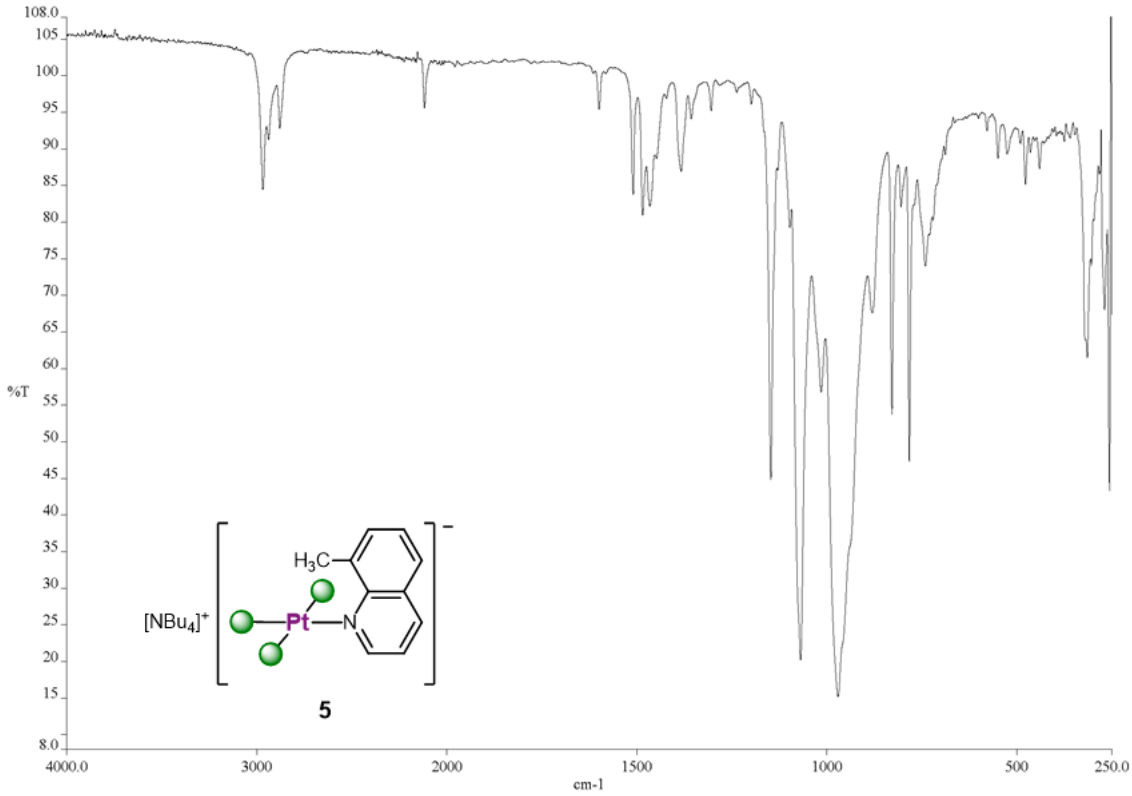

Figure S20. IR spectrum of compound **5**.

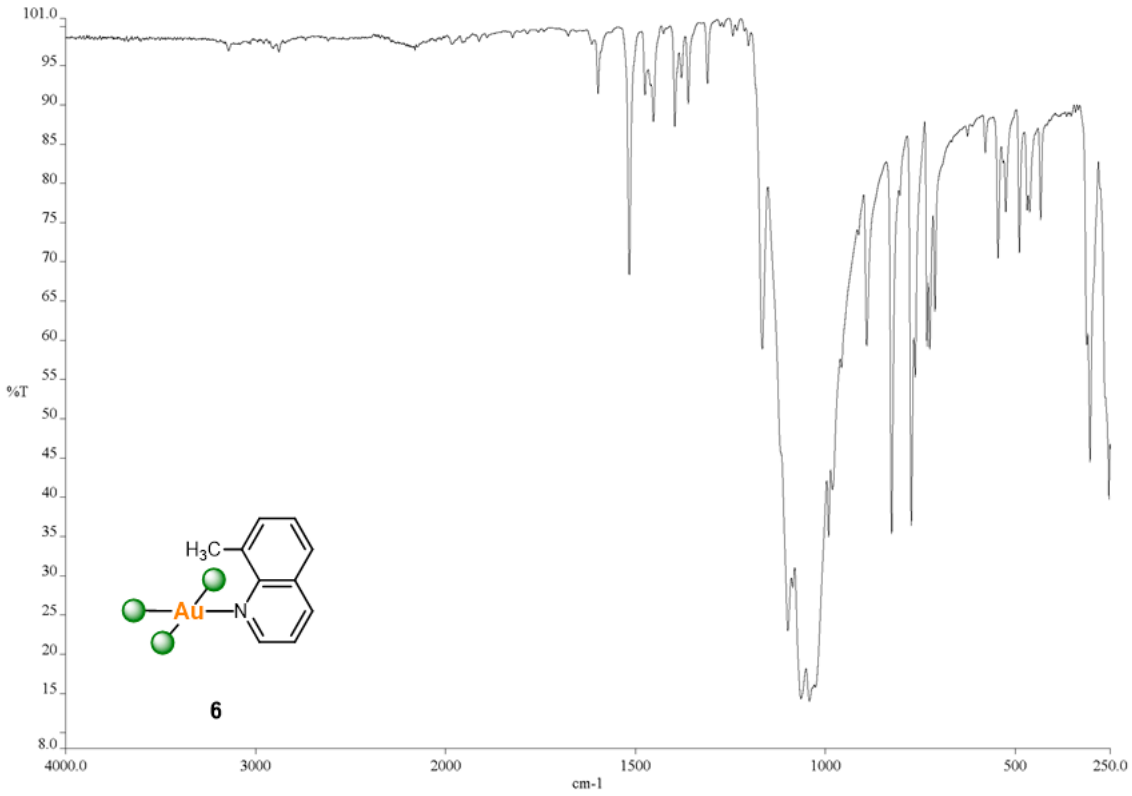

Figure S21. IR spectrum of compound **6**.

2. Crystal Data and Structure Refinement

Crystal data and other details of the structure analyses are presented in Tables S1–S5. Suitable crystals for X-ray diffraction studies were obtained as indicated in the corresponding experimental entry. Crystals were mounted at the end of a quartz fibre. The radiation used in all cases was graphite monochromated Mo-Kα (λ = 71.073 pm). X-ray intensity data were collected on an Oxford Diffraction Xcalibur diffractometer. The diffraction frames were integrated and corrected from absorption by using the CrysAlis RED program.[S5] Data collection was performed at 100 K.

The structures were solved by Patterson and Fourier methods and refined by full-matrix least squares on F^2 with SHELXL.[S6] All non-H atoms were assigned anisotropic displacement parameters and refined without positional constraints. The positions of the H atoms were constrained to idealised geometries and assigned isotropic displacement parameters equal to 1.2 or 1.5 times the U_{iso} values of their respective parent atoms, except as noted below. All CH_3 groups were allowed to freely rotate around the C–C bond. In the structures of **2** and **3**·OEt_2, the position of the O***H*** atom was found in the electron density maps and allowed to refine freely both in position and in thermal parameter. For **3**·OH_2, the positions of all three O***H*** atoms were found in the electron density maps and later refined with 1.2 times U_{iso} values of their parent O atoms at a fixed O–H distance of 82 pm (DFIX). In the structure of **5**, the CF_3 groups show rotational disorder, which was modelled with two sets of F atoms in equally occupied positions. Constrains in the U_{iso} values of the F atoms and in the C–F distance were added. Full-matrix least-squares refinement of the models against F^2 converged to final residual indices given in Tables S1–S5.

Table S1. Crystal data and structure refinement for compound **2**

formula	$C_{29}H_{45}F_9N_2OPt$
M_t [g mol^{-1}]	803.76
T [K]	100(1)
λ [pm]	71.073
crystal system	monoclinic
space group	$P2_1$
a [pm]	806.37(2)
b [pm]	1657.56(3)
c [pm]	1215.07(2)
β [°]	103.532(2)
V [nm^3]	1.57897(5)
Z	2
ρ [g cm^{-3}]	1.691
μ [mm^{-1}]	4.522
F(000)	800
2θ range [°]	9.1–58.7
no. of reflns colltd	17746
no. of unique reflns	7229
R_{int}	0.0374
R indices [$I > 2\sigma(I)$][a]	
R_1	0.0303
wR_2	0.0678
R indices (all data)	
R_1	0.0333
wR_2	0.0710
goodness-of-fit[b] on F^2	1.025
Abs. struct. param.	−0.020(5)
CCDC no.	2040138

[a] $R_1 = \sum(|F_o| - |F_c|) / \sum|F_o|$; $wR_2 = [\sum w(F_o^2 - F_c^2)^2 / \sum w(F_o^2)^2]^{1/2}$.
[b] Goodness-of-fit = $[\sum w(F_o^2 - F_c^2)^2 / (n_{obs} - n_{param})]^{1/2}$.

Table S2. Crystal data and structure refinement for compound **3**·OEt_2

formula	$C_{12}H_7AuF_9NO·OEt_2$
M_t [g mol^{-1}]	623.27
T [K]	100(1)
λ [pm]	71.073
crystal system	monoclinic
space group	$P2_1/c$
a [pm]	1360.93(5)
b [pm]	1029.74(3)
c [pm]	1436.95(4)
β [°]	98.813(3)
V [nm^3]	1.98998(11)
Z	4
ρ [g cm^{-3}]	2.080
μ [mm^{-1}]	7.486
F(000)	1184
2θ range [°]	8.4–59.5
no. of reflns colltd	19835
no. of unique reflns	5175
R_{int}	0.0412
R indices [$I > 2\sigma(I)$][a]	
R_1	0.0285
wR_2	0.0575
R indices (all data)	
R_1	0.0373
wR_2	0.0620
goodness-of-fit[b] on F^2	1.045
CCDC no.	2040139

[a] $R_1 = \sum(|F_o| - |F_c|) / \sum|F_o|$; $wR_2 = [\sum w(F_o^2 - F_c^2)^2 / \sum w(F_o^2)^2]^{1/2}$.
[b] Goodness-of-fit = $[\sum w(F_o^2 - F_c^2)^2 / (n_{obs} - n_{param})]^{1/2}$.

Table S3. Crystal data and structure refinement for compound **3**·OH_2

formula	$C_{12}H_7AuF_9NO·OH_2$
M_t [g mol^{-1}]	567.17
T [K]	100(1)
λ [pm]	71.073
crystal system	triclinic
space group	$P\bar{1}$
a [pm]	805.27 (1)
b [pm]	948.58(2)
c [pm]	1040.80(2)
α [°]	95.525(2)
β [°]	98.451(1)
γ [°]	100.077(2)
V [nm^3]	0.76816(2)
Z	2
ρ [g cm^{-3}]	2.452
μ [mm^{-1}]	9.683
F(000)	528
2θ range [°]	6.0–56.8
no. of reflns colltd	29617
no. of unique reflns	3519
R_{int}	0.0404
R indices [$I > 2\sigma(I)$][a]	
R_1	0.0186
wR_2	0.0431
R indices (all data)	
R_1	0.0192
wR_2	0.0434
goodness-of-fit[b] on F^2	1.156
CCDC no.	2040140

[a] $R_1 = \sum(|F_o| - |F_c|) / \sum|F_o|$; $wR_2 = [\sum w(F_o^2 - F_c^2)^2 / \sum w(F_o^2)^2]^{1/2}$.

[b] Goodness-of-fit = $[\sum w(F_o^2 - F_c^2)^2 / (n_{obs} - n_{param})]^{1/2}$.

Table S4. Crystal data and structure refinement for compound **5**

formula	$C_{29}H_{45}F_9N_2Pt$
M_t [g mol^{-1}]	787.76
T [K]	100(1)
λ [pm]	71.073
crystal system	monoclinic
space group	$P2_1/c$
a [pm]	1094.40(2)
b [pm]	1761.47(4)
c [pm]	1657.47(3)
β [°]	101.576(2)
V [nm^3]	3.13020(10)
Z	4
ρ [g cm^{-3}]	1.672
μ [mm^{-1}]	4.557
F(000)	1568
2θ range [°]	8.8–58.6
no. of reflns colltd	34391
no. of unique reflns	7661
R_{int}	0.0393
R indices [$I > 2\sigma(I)$][a]	
R_1	0.0654
wR_2	0.1634
R indices (all data)	
R_1	0.0746
wR_2	0.1697
goodness-of-fit[b] on F^2	1.070
CCDC no.	2040141

[a] $R_1 = \sum(|F_o| - |F_c|) / \sum|F_o|$; $wR_2 = [\sum w(F_o^2 - F_c^2)^2 / \sum w(F_o^2)^2]^{1/2}$.
[b] Goodness-of-fit = $[\sum w(F_o^2 - F_c^2)^2 / (n_{obs} - n_{param})]^{1/2}$.

Table S5. Crystal data and structure refinement for compound **6**

formula	$C_{13}H_9AuF_9N$
M_t [g mol^{-1}]	547.18
T [K]	100(1)
λ [pm]	71.073
crystal system	monoclinic
space group	$P2_1/c$
a [pm]	1152.07(2)
b [pm]	1538.69(2)
c [pm]	823.76(2)
β [°]	96.571(1)
V [nm^3]	1.45067(4)
Z	4
ρ [g cm^{-3}]	2.505
μ [mm^{-1}]	10.240
F(000)	1016
2θ range [°]	4.8–56.9
no. of reflns colltd	27537
no. of unique reflns	3341
R_{int}	0.0341
R indices [$I > 2\sigma(I)$][a]	
R_1	0.0204
wR_2	0.0403
R indices (all data)	
R_1	0.0235
wR_2	0.0413
goodness-of-fit[b] on F^2	1.123
CCDC no.	2040142

[a] $R_1 = \sum(|F_o| - |F_c|) / \sum|F_o|$; $wR_2 = [\sum w(F_o^2 - F_c^2)^2 / \sum w(F_o^2)^2]^{1/2}$.
[b] Goodness-of-fit = $[\sum w(F_o^2 - F_c^2)^2 / (n_{obs} - n_{param})]^{1/2}$.

3. Computational Details

Quantum mechanical calculations were performed with the Gaussian09 package[S7] at the DFT/M06 level of theory.[S8] Non-metal atoms (H, C, N, O and F) were described with a 6-31G** basis set.[S9,S10] In turn, the SDD basis set and its corresponding effective core potentials (ECPs) were used to describe the metal atoms (Pt and Au)[S11] augmented by additional sets of f-type functions.[S12] The potential energy surfaces of the complexes under study have been examined at this level of theory and their geometries have been optimized in the gas phase with no symmetry restrictions, except as noted below. Frequency calculations have been performed for every stationary point in order to identify them as minima or transition states. Relevant experimental and calculated geometric parameters are compared in Table S6. The model complexes **7** and **8** have virtual C_s symmetry when freely optimized. In order to ease the analysis of their electronic structures, the geometries were re-optimized under imposed C_s symmetry. The resulting geometries **7**-C_s and **8**-C_s (Figure 6) lay very close in energy to the former ones ($\Delta E < 1$ kcal mol^{-1}). Atomic coordinates for all the optimized structures are included as a separate *.xyz* file.

Topological analyses of the electron density distribution functions $\rho(\mathbf{r})$ were performed for compounds **1**–**4** as well as for the adduct **3**·OEt_2 using the AIMAll program package[S13] based on the extended wave functions obtained by M06 calculations. The AIM extended wave-function format allows QTAIM analyses of molecular systems containing heavy atoms described with ECPs. The topological features of especially relevant critical points (CP) are given in Table 2. Important cross sections in the contour-line $\nabla^2\rho(\mathbf{r})$ maps are shown in Figures 5 (**1**–**4**) and S22 (**3**·OEt_2). The electronic structures and MO compositions of **7**-C_s and **8**-C_s were analyzed (Figure 7) by using Chemissian software.[S14]

Table S6. Comparison of the most relevant geometric parameters of the structurally characterized derivatives containing the isoelectronic $(CF_3)_3M$ fragments in this work (M = Pt, Au; E = C, O) with those calculated at the DFT/M06 level of theory.[a]

Compound	M–C (pm)[b]	av- M–C_2 (pm)[c]	M–N (pm)	M···E (pm)	E–H (pm)	M···H (pm)	∑∠ (deg)[d]
$[NBu_4][(CF_3)_3Pt(hq')]$ (**2**)	202.0(6)	206.6(7)	213.2(5)	297.2(5)	97(9)	205(9)	360.1(3)
2-DFT	200.5	208.5	220.5	300.5	99.5	205.5	360
$(CF_3)_3Au(hq{\cdot}OEt_2)$ (**3**·OEt_2)	202.3(4)	207.6(4)	210.9(3)	268.8(3)	77(5)	—[e]	360.02(16)
3·OEt_2-DFT	204.5	210.5	219	264	99.5	—[e]	360
$[NBu_4][(CF_3)_3Pt(mq)]$ (**5**)	199.9(8)	205.7(8)	212.7(7)	309(1)	98[f]	273[f,g]	360.3(3)
5-DFT	200	208.5	221.5	315	109.5	273[g]	360
$(CF_3)_3Au(mq)$ (**6**)	202.9(3)	208.9(3)	211.2(3)	305.1(3)	98[f]	267[f,g]	360.04(13)
6-DFT	205	211	219	306	109.5	270[g]	360

[a] Atomic coordinates of the optimized structures are given in a separate *.xyz* file. [b] The M–C distance *trans* to the neutral N-donor ligand is here indicated. [c] Average of the two independent M–C bond lenghts in *trans* arrangement. [d] Summation of all adjacent E–M–E' angles as a measure of planarity. [e] The O–H unit interacts with a Et_2O molecule, where the Et_2O···H–O angle amounts 178(6)° (exp.) *vs*. 159° (theor.), and the O···O' separation is 263.6(4) pm (exp.) *vs*. 258 pm (theor.). [f] No estimated experimental error is here indicated because the H position was refined under constraints. [g] The closest M···H distance is here indicated.

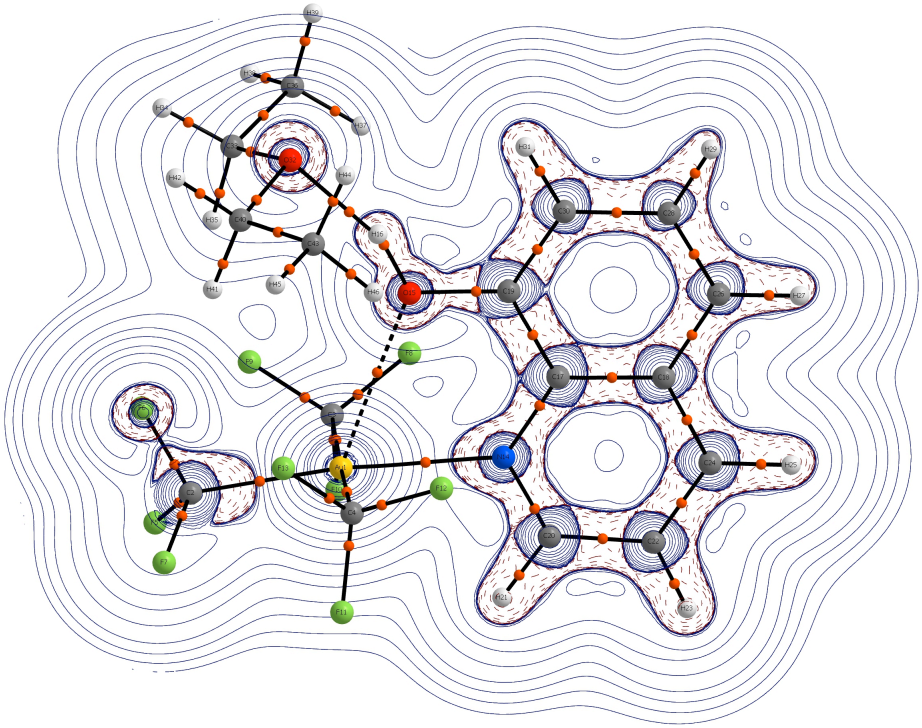

Figure S22. 2D contour-line $\nabla^2\rho(\mathbf{r})$ diagram obtained from QTAIM analysis of the optimized **3**·OEt_2 adduct. The cross section contains the Au, O and N atoms. Bond critical points (orange spheres) and bond paths (black straight lines) are shown as obtained using weak-CP (0.03) and non-CP (0.02) thresholds.

4. Notes and References

S1 S. Martínez-Salvador, J. Forniés, A. Martín, B. Menjón and I. Usón, *Chem. Eur. J*., 2013, **19**, 324.

S2 A. Pérez-Bitrián, M. Baya, J. M. Casas, L. R. Falvello, A. Martín and B. Menjón, *Chem. Eur. J*., 2017, **23**, 14918.

S3 The quaternary carbon atoms C8, C9 and C10 could not be located.

S4 The quaternary carbon atoms C8 and C10 could not be located.

S5 CrysAlis RED: *Program for X-ray CCD camera data reduction*, Oxford Diffraction Ltd., Oxford, UK, 2008.

S6 SHELXL Version 2014/8: G. M. Sheldrick, *Acta Crystallogr. Sect. C*, 2015, **71**, 3.

S7 M. J. Frisch, G. W. Trucks, H. B. Schlegel, G. E. Scuseria, M. A. Robb, J. R. Cheeseman, G. Scalmani, V. Barone, B. Mennucci, G. A. Petersson, H. Nakatsuji, M. Caricato, X. Li, H. P. Hratchian, A. F. Izmaylov, J. Bloino, G. Zheng, J. L. Sonnenberg, M. Hada, M. Ehara, K. Toyota, R. Fukuda, J. Hasegawa, M. Ishida, T. Nakajima, Y. Honda, O. Kitao, H. Nakai, T. Vreven, J. A. Montgomery, Jr., J. E. Peralta, F. Ogliaro, M. Bearpark, J. J. Heyd, E. Brothers, K. N. Kudin, V. N. Staroverov, T. Keith, R. Kobayashi, J. Normand, K. Raghavachari, A. Rendell, J. C. Burant, S. S. Iyengar, J. Tomasi, M. Cossi, N. Rega, J. M. Millam, M. Klene, J. E. Knox, J. B. Cross, V. Bakken, C. Adamo, J. Jaramillo, R. Gomperts, R. E. Stratmann, O. Yazyev, A. J. Austin, R. Cammi, C. Pomelli, J. W. Ochterski, R. L. Martin, K. Morokuma, V. G. Zakrzewski, G. A. Voth, P. Salvador, J. J. Dannenberg, S. Dapprich, A. D. Daniels, O. Farkas, J. B. Foresman, J. V. Ortiz, J. Cioslowski and D. J. Fox: *Gaussian 09, Revision D.01*; Gaussian, Inc., Wallingford CT, 2013.

S8 Y. Zhao and D. G. Truhlar, *Theor. Chem. Acc*., 2008, **120**, 215.

S9 P. C. Hariharan and J. A. Pople, *Theor. Chim. Acta*, 1973, **28**, 213.

S10 M. M. Francl, W. J. Pietro, W. J. Hehre, J. S. Binkley, M. S. Gordon, D. J. DeFrees and J. A. Pople, *J. Chem. Phys*., 1982, **77**, 3654.

S11 D. Andrae, U. Häußermann, M. Dolg, H. Stoll and H. Preuß, *Theor. Chim. Acta*, 1990, **77**, 123.

S12 A. W. Ehlers, M. Böhme, S. Dapprich, A. Gobbi, A. Höllwarth, V. Jonas, K. F. Köhler, R. Stegmann, A. Veldkamp and G. Frenking, *Chem. Phys. Lett*., 1993, **208**, 111.

S13 A. Todd and T. K. Keith: AIMAll, version 13.05.06; Gristmill Software, Overland Park KS, 2013.

S14 L. V. Skripnikov: Chemissian, Version 3.3, *Visualization computer program*, 2012, www.chemissian.com